Stability Analysis of the ITER PF Coils

Laura Savoldi Richard, Denis Bessette, and Roberto Zanino

***Abstract*—The 1D stability analysis of a subset of the International Thermonuclear Experimental Reactor (ITER) Poloidal Field (PF) coils, namely PF2, PF3, PF5, is presented, using the Mithrandir code. Different combinations of lengths and durations are considered for the stability disturbance, applied to the superconducting cable during the most critical operating condition. In all cases the computed energy margin is well above the presently expected disturbance on the coils.**

***Index Terms*—Fusion reactors, ITER, stability, superconducting magnets.**

I. Introduction

THE documentation of the International Thermonuclear Experimental Reactor (ITER) conductors is being updated with respect to the last version, dating now back to 2001 [1]. As a part of that effort, the stability analysis of the whole set of coils—Toroidal Field (TF), Poloidal Field (PF) and Central Solenoid (CS)—is being performed at Politecnico di Torino with updated tools, scenarios, conductor designs.

The general approach we use is follows: the most critical conductor in the winding pack, as well as the most critical location along it, from the point of view of the temperature margin, is identified by a global analysis using the Vincenta code [2], which also provides the initial and boundary conditions for the stability study, as well as the heat load distribution on the conductor due to AC losses, nuclear heating and thermal conduction/radiation. With this input, we perform a local 1D stability analysis using the Mithrandir code [3], restricted to the most critical conductor; a much finer grid can then be afforded than by Vincenta, allowing capturing the details of normal zone initiation and possible recovery to the superconducting state.

In [4] the results of the stability analysis for the TF coils were presented. Here, the stability analysis of the reference NbTi conductors for the PF2, 3, 5 coils is presented. Different combinations of lengths (1 cm to 1 m) and durations (1 ms to 100 ms) are considered for the stability disturbance, applied to the superconducting cable during the most critical operating condition. The independence of the results from the grid size and time step is carefully verified, as well as their parametric sensitivity to the choice of the heat transfer coefficient between strands and helium. Finally, some details of the thermal-hydraulic transient are discussed, in order to explain how the decision between quench and recovery is taken for the different disturbance scenarios.

Manuscript received August 23, 2008. First published June 10, 2009; current version published July 15, 2009. This work was supported in part by the European Fusion Development Agreement (EFDA) and by the Italian Ministry for University and Research (MUR). LSR is also a grateful recipient of a Politecnico di Torino fellowship "Giovani ricercatori".

L. Savoldi Richard and R. Zanino are with Dipartimento di Energetica, Politecnico, Torino I-10129, Italy (e-mail: laura.savoldi@polito.it).

D. Bessette is with ITER Organization, Cadarache, France (e-mail: denis.bessette@iter.org).

Color versions of one or more of the figures in this paper are available online at http://ieeexplore.ieee.org.

Digital Object Identifier 10.1109/TASC.2009.2018752

TABLE I
PF Reference NbTi Conductor Data

	PF2, PF3	PF5
# of strands (SC, Cu)	864, 30	1080, 36
∅ strands (SC) (mm)	0.73	0.72
Cu : non-Cu (SC strands)	6.9	4.4
RRR	150	
Cabling pattern	((3×3×4+1) ×4+1)×6	((3×3×4+1) ×5+1)×6
Cosθ	0.95	
Void fraction	34.2%	34.3%
∅ central channel (ID × OD) (mm)	10 × 12	
Central channel nominal perforation	0.15	
Jacket cross section (mm^2)	1822.02	1736.99
Jacket material	SS	

II. Definition of the Input

A. Conductor Data

The major input parameters concerning the reference conductors are summarized in Table I below. The same strand critical properties are assumed in all coils, as given in [5], with conductor $\mathrm{n-value} = 40$.

B. Input From Global Vincenta Analysis

The most critical location in time ($\mathrm{t} = \mathrm{t}^*$) and space ($\mathrm{x} = \mathrm{x}^*$) *from the point of view of the temperature margin* and, as such, most suitable for the localization of the stability disturbance, is identified first. Several consecutive plasma pulses are carried out until quasi-repetitive operating conditions are achieved along the coil in terms of temperature, pressure and mass flow rate, during the 4th pulse, leading to $\mathrm{t}^* \sim 5990$ s, 5930 s and 5500 s, respectively, for PF2, PF3, PF5 (i.e., basically at the peak current/field instants in Fig. 1 below); the center of the disturbance is then localized where the temperature margin at t^* is minimum, that is $\mathrm{x}^* \sim 36.9$ m, 47.9 m, 24.3 m, for PF2, PF3, PF5 (i.e., basically where the field is maximum in Fig. 2 below), along pancake # 5, 8, 10, respectively.

C. Other Input Assumptions

For the friction factors in the cable region and central channel the correlations reported in [6], have been used.

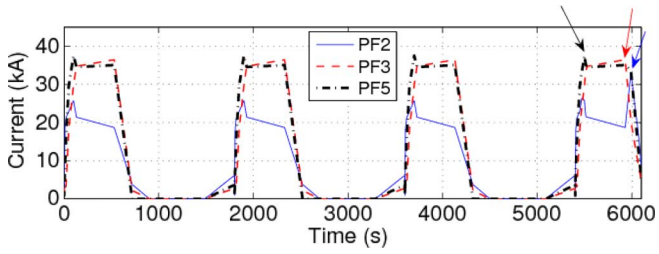

Fig. 1. Current scenarios for the first 4 pulses in PF2, 3, 5 (The dwell and current ramp-up to initial magnetization phases of the 4th pulse omitted, as the temperature margin is anyway higher for those periods of time.)

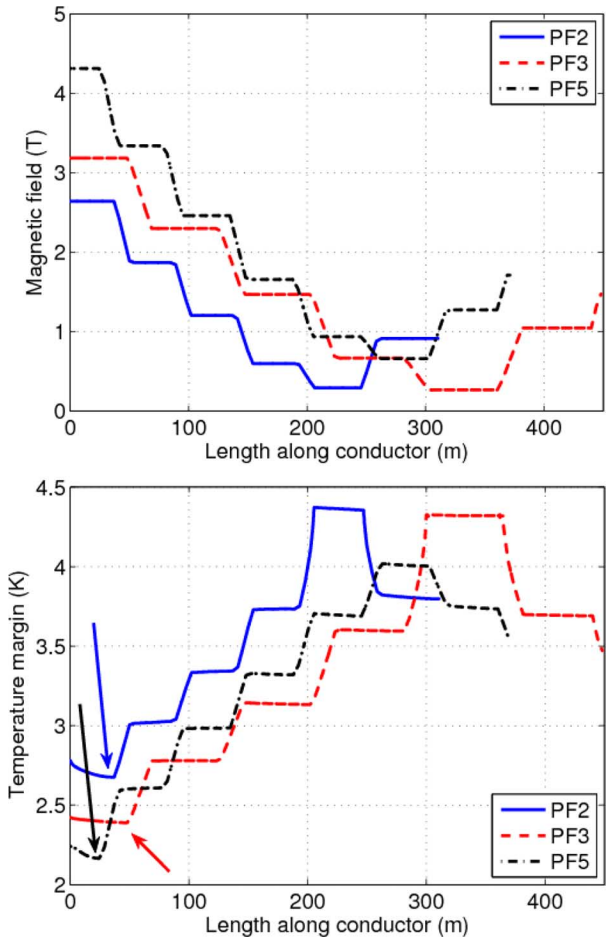

Fig. 2. Magnetic field (top) and corresponding temperature margin distribution (bottom) along the most critical pancake for PF2 (solid), PF3 (dashed), PF5 (dash-dotted). The minimum location on each curve is indicated by arrows.

The following heat transfer coefficients have been assumed in the reference calculation: Dittus-Boelter correlation between strands and helium (no transient component) as well as between jacket and helium, series of thermal resistors between bundle helium and hole helium (Dittus-Boelter bundle side, heat conduction through spiral where present, Dittus-Boelter hole side), while the direct contact heat transfer between strands and jacket is neglected.

The maximum (fixed) time step Δt and grid size Δx that can be used for the analysis of each disturbance have been determined by a suitable numerical convergence study, see Fig. 3 below. The above-mentioned grid size refers to a zone around

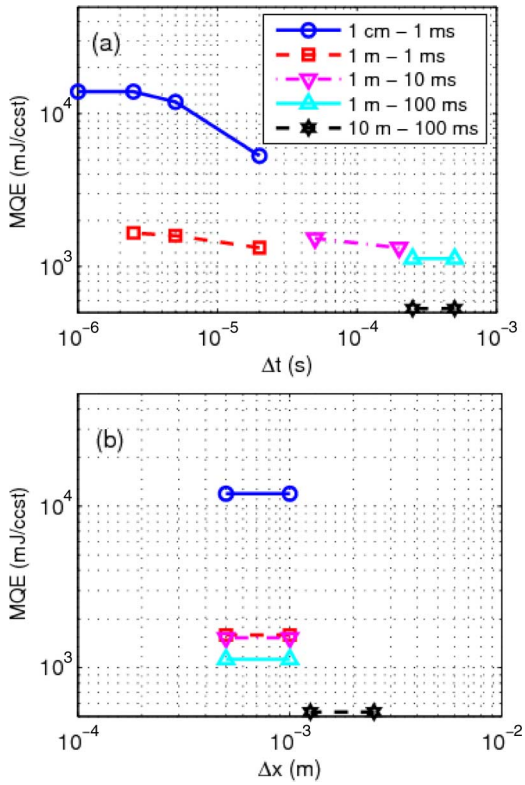

Fig. 3. Summary of results of numerical convergence studies in time (a) and space (b) for the different disturbances.

TABLE II
DISTURBANCE SCENARIOS

L (m)	τ (ms)
0.01	1
1	1
1	10
1	100
10	100

x^*, whereas in the rest of the conductor a mesh size ~100 times larger is typically used.

D. Disturbance Scenarios

The disturbance scenarios (duration τ and length L of the square wave heat pulses applied to the conductors at t^*, centered around x^*), are summarized in Table II. The disturbances are of various natures, including short duration/short length (1 cm/1 ms) pulses for the simulation of a disturbance of mechanical origin and long duration/long length (10 m, 0.1 s) pulses for the simulation of a disturbance of electromagnetic origin.

The stability threshold is automatically searched by Mithrandir simulations via a scan of amplitudes Q (W/m) for each disturbance analysed and it is bracketed by a maximum recovery energy (MRE) and by a minimum quench energy (MQE), given in terms of energies E per cubic centimeter of strand, $E = Q\tau/A_{st}$. By definition, a transient is assumed to

TABLE III
COMPUTED MQE AND MRE ($\mathrm{mJ/ccst^*}$)

	B (T)	I (kA)	A_{st} (mm^2)	L (m) →	0.01		1		10
				τ (ms) →	1	1	10	100	100
PF2	2.64	33.2	376	MRE	17265	1859	1793	1262	930
				MQE	17929	1926	1859	1328	996
PF3	3.18	36.5	376	MRE	13281	1594	1461	1062	600
				MQE	13945	1660	1527	1129	664
PF5	4.31	37.6	458	MRE	9285	873	928	710	437
				MQE	9831	928	983	765	492

* $\mathrm{ccst} = \mathrm{cm^3}$ of strand

end with a recovery, as soon as the maximum electric field after the end of the pulse falls/stays below 10 $\mu\mathrm{V/m}$, i.e. below the $\mathrm{T_{CS}}$, while it is assumed to end with a quench as soon as a voltage larger than 0.1 V is computed along the entire pancake.

III. Results and Analysis

A. Summary

The results of our analysis for the whole set of disturbances and the whole set of conductor/coil are summarized in terms of MQE/MRE in Table III below.

It may be noted that the MQE directly depends, as expected for a given disturbance, on the temperature margin of the particular conductor/coil, see Fig. 2. For a given conductor/coil, the MQE increases in most cases when going from disturbances of large duration and length to shorter disturbances (in space and/or time).

If compared with preliminary estimates of the energy per $\mathrm{cm^3}$ of strand (ccst) deposited by mechanical disturbance [5], and/or plasma disruption [7], performed in the past, the PF2, 3, 5 conductors/coils are predicted here to be stable by a large margin.

B. Detailed Analysis for the PF3 Conductor/Coil

For the intermediate case of the PF3, see Table III, we provide here some insight and comments on the evolution of the thermal-hydraulic transient after the disturbance is applied and in particular on how this detailed dynamics, simulated by the Mithrandir code, leads to the decision on quench/recovery. Also the parametric effect of different heat transfer coefficients between strands and helium will be discussed.

In the first place, we show in Fig. 3 the result of the space and time numerical convergence study performed for PF3. The results above and below have been obtained with $\Delta\mathrm{t}$ and $\Delta\mathrm{x}$ such as to give mesh-independent results. It may be seen that up to more than 10^2 steps are needed to resolve the pulse in time while as little as 10 nodes are sufficient to resolve the pulse in space.

We now consider the details of the computed thermal-hydraulic transient following the short (0.01 m/1 ms) disturbance and compare with the transients following the (1 m/100 ms). In both cases an important role is obviously played by the time scale $\tau_{\mathrm{St-He}}$ over which the helium becomes thermally coupled to the strands. From the 0D transient energy balance

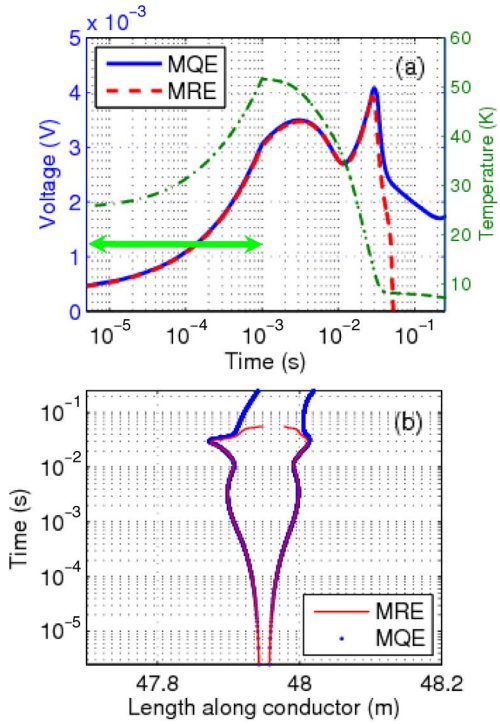

Fig. 4. Results of (1 cm/1 ms) pulse analysis: (a) evolution of voltage for MQE (solid) and MRE input (dashed), evolution of strand temperature in the center of the initially heated region for MQE (dash-dotted)—the thick line indicates the end of the pulse; (b) normal zone propagation in characteristics plane for MQE (dots) and MRE (solid).

$(\rho \mathrm{C_p})_{\mathrm{st}} \mathrm{A_{st}} \partial \mathrm{T_{St}}/\partial \mathrm{t} \sim \mathrm{H\,P}(\mathrm{T_{He}} - \mathrm{T_{St}})$ this can be roughly estimated as $\tau_{\mathrm{st-He}} \sim [\mathrm{T_{st}}(\mathrm{t}+\tau) - \mathrm{T_{st}}(\mathrm{t})]/[\mathrm{T_{st}}(\mathrm{t}+\tau) - \mathrm{T_{He}}(\mathrm{t}+\tau)]^*(\rho \mathrm{C_p})_{\mathrm{st}} \mathrm{A_{st}}/(\mathrm{H\,P}) \sim (1)\ 10^4\ 400\ 10^{-6}/(500\ 2) \sim$ 1–10 ms.

In the (1 cm/1 ms) case $\tau <\sim \tau_{\mathrm{St-He}}$, therefore the voltage, the temperature $\mathrm{T}(\mathrm{x}^*)$ and the normal zone (NZ) length evolve adiabatically and monotonically during the heating, see Fig. 4(a). Shortly after the end of the heating the voltage starts decreasing as the normal zone contracts because of coupling to the cold helium at the NZ boundary, see Fig. 4(b). Then, after sufficient hot helium starts expanding away from the originally heated region, the NZ starts propagating upstream and downstream until the downstream (background) flow of cold helium pushes it back again, leading to a significant drop of the voltage, see again Fig. 4(a). Only at this time, i.e. on a

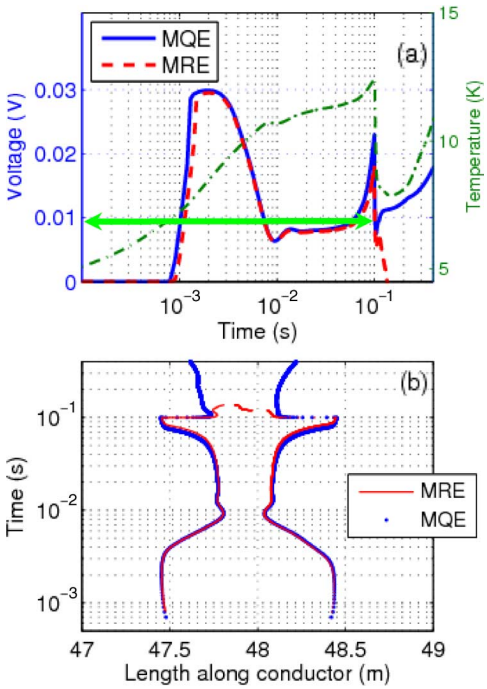

Fig. 5. Results of (1 m/100 ms) pulse analysis: (a) evolution of voltage for MQE (solid) and MRE input (dashed), evolution of strand temperature in the center of the initially heated region for MQE (dash-dotted)—the thick line indicates the end of the pulse; (b) normal zone propagation in characteristics plane for MQE (dots) and MRE (solid).

much longer time scale than τ, the system decides between quench and recovery. Note that $\mathrm{T}(\mathrm{x}^*)$ monotonically decreases after the pulse as the NZ is being carried downstream by the background flow, even in the case of the quench.

In the (1 m/100 ms) case, on the contrary, $\tau \gg \tau_{\mathrm{St-He}}$, therefore the voltage starts decreasing already during the pulse, see Fig. 5(a), again because of coupling to the cold helium which leads to a contraction of the NZ, see Fig. 5(b). Then, similarly to the case above, expansion of hot helium leads to propagation of the quench upstream and downstream until both temperature and voltage collapse at the end of the pulse. Here, the decision between quench and recovery is quickly taken, i.e., on a time scale of the same order of τ, and in the case of the quench $\mathrm{T}(\mathrm{x}^*)$ quickly starts increasing again.

Part of the features discussed above is related to the dependence of the DB heat transfer coefficient on the Reynolds number (effect of the induced flow). The parametric effect of different heat transfer coefficients between strands and helium on the stability margin (MQE) has also been investigated. The heat transfer coefficient has been varied in the range between 500 $\mathrm{W/m^2K}$ and 5000 $\mathrm{W/m^2K}$, showing a very limited impact on the stability margin, as opposed to what happened for the TF coils [4]. This is due to the fact that the PF conductors, in view of their very high temperature margin, are already in the well-cooled region with 500 $\mathrm{W/m^2K}$, therefore their stability is not significantly affected by a further increase of the heat transfer coefficient.

IV. Conclusions and Perspective

The ITER PF conductor documentation has been updated with respect to the stability of PF2, 3, 5. In all cases the computed energy margin is well above the presently expected disturbance on the coils. We plan to complete the analysis of the PF coils by including the PF6.

The same methodology shall eventually be applied to the stability analysis of the CS conductors and coil, thus completing the original task of updating the documentation for the whole ITER magnet system.

References

[1] ITER Design Description Document. Magnet: Section 1: Engineering Description, N 11 DDD 178 04-06-04 R 0.4 2004.
[2] D. Bessette, N. Shatil, and E. Zapretilina, "Simulation of the ITER toroidal field coil operation with the VINCENTA code," *IEEE Trans. Appl. Supercond.*, vol. 16, pp. 795–799, 2006.
[3] R. Zanino, S. De Palo, and L. Bottura, *J. Fus. Energy*, vol. 14, pp. 25–40, 1995.
[4] L. Savoldi Richard and R. Zanino, "Stability analysis of the ITER TF conductor," *Adv. Cryo Eng.*, vol. 52, pp. 1269–1276, 2008.
[5] Magnet Superconducting and Electrical Design Criteria (MSEC), N 11 MA 2 R 0.1 2004.
[6] S. Nicollet *et al.*, "Dual channel cable in conduit thermohydraulics: Influence of some design parameters," *IEEE Trans. Applied Supercond.*, vol. 10, pp. 1102–1105, 2000.
[7] ITER Design Description Document. DDD1 Magnet: Section 2: Performance Analysis, 2.1 Conductor Design Analysis, N 11 DDD 156 01-07-13 R 0.1 2001.